

# Damping of high-temperature shape memory alloys

Kirsten P. Duffy\*<sup>a</sup>, Santo A. Padula, II<sup>b</sup>, Daniel A. Scheiman<sup>c</sup>

<sup>a</sup>Univ. of Toledo/NASA Glenn Research Center, 21000 Brookpark Rd., Cleveland, OH, USA 44135

<sup>b</sup>NASA Glenn Research Center, 21000 Brookpark Rd., Cleveland, OH, USA 44135

<sup>c</sup>ASRC/NASA Glenn Research Center, 21000 Brookpark Rd., Cleveland, OH, USA 44135

## ABSTRACT

Researchers at NASA Glenn Research Center have been investigating high temperature shape memory alloys as potential damping materials for turbomachinery rotor blades. Analysis shows that a thin layer of SMA with a loss factor of 0.04 or more would be effective at reducing the resonant response of a titanium alloy beam. Two NiTiHf shape memory alloy compositions were tested to determine their loss factors at frequencies from 0.1 to 100 Hz, at temperatures from room temperature to 300°C, and at alternating strain levels of 34-35x10<sup>-6</sup>. Elevated damping was demonstrated between the M<sub>s</sub> and M<sub>f</sub> phase transformation temperatures and between the A<sub>s</sub> and A<sub>f</sub> temperatures. The highest damping occurred at the lowest frequencies, with a loss factor of 0.2-0.26 at 0.1 Hz. However, the peak damping decreased with increasing frequency, and showed significant temperature hysteresis in heating and cooling.

**Keywords:** High-temperature, shape memory alloy, damping, aircraft engine blades, NiTiHf

## 1. INTRODUCTION

### 1.1 Turbomachinery blade damping

As part of the Fundamental Aeronautics program, researchers at NASA Glenn Research Center (GRC) are developing new damping technologies to alleviate excessive vibratory stresses that lead to high cycle fatigue failures in aircraft engine components. Newer high-performance turbomachinery blade designs have led to decreased blade damping and higher vibratory stresses<sup>1</sup>. This increases design and maintenance costs, but also can cause component failure. Designing damping treatments for rotating blades in an extreme engine environment is difficult because temperatures and centrifugal accelerations can be very high. Since a damping treatment must not affect the aerodynamics of the blade, it must be internal to the blade, out of the air stream, or applied to the blade surface in a thin layer. In addition to that, it is extremely challenging to design damping that can withstand the harsh engine environment and still remain both cost-effective and easy to produce.

Several damping methods have been investigated at NASA GRC for use in aircraft engines, including viscoelastic damping, impact damping, plasma sprayed damping coatings, and shunted piezoelectric damping. The current effort seeks to investigate the damping characteristics of high temperature shape memory alloys (HTSMAs) that are being developed by NASA GRC to see if these materials may be a viable alternative.

### 1.2 Shape memory alloy damping

Elevated damping in shape memory alloys (SMAs) occurs when energy is dissipated during the solid-state phase transformation. When the material is in the austenite state slightly above the A<sub>f</sub> temperature, application of external stress can induce the martensite phase. Large recoverable strains with significant hysteresis can be observed, depending on the level of stress applied. Figure 1 shows that even at an operating temperature T<sub>op</sub> above the austenite finish temperature A<sub>f</sub>, applied stress above the threshold stress level  $\sigma_t$  can induce phase transformation within the alloy. In general, the amount of damping observed will depend on the temperature, alternating stress level, steady-state stress level, and frequency.

\*Kirsten.P.Duffy@nasa.gov; phone 1 216 433-3880

Sherwin and Ulmer<sup>2</sup> hold a patent for a concept where a SMA could be used to suppress aircraft engine blade vibrations. In this concept, SMA patches are placed on the blade at high vibratory stress locations, where the maximum operating temperature is similar to the martensite-to-austenite transformation temperature. The vibratory stresses imparted to the blade cause these patches to deform, initiating the phase transformation that leads to increased damping.

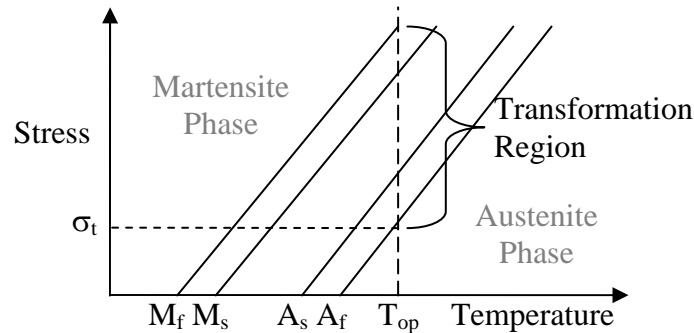


Fig. 1. Stress versus temperature for a shape memory alloy – operating temperature  $T_{op}$ .  $M_f$  – martensite finish temperature,  $M_s$  – martensite start temperature,  $A_s$  – austenite start temperature,  $A_f$  – austenite finish temperature,  $\sigma_t$  – threshold stress.

In recent years, researchers have reported high damping values for SMAs. This high damping has been associated with the phase transformation that occurs in these alloys. Van Humbeeck<sup>3</sup> describes the conclusions of several studies of SMAs, particularly NiTi, showing damping can be an order of magnitude higher than typical metals. An amplitude-dependence was shown especially at low strains (below  $10^{-6}$ ) and at high strains (above about  $10^{-5}$ ), with best damping occurring at the higher strain levels. Alloy composition and thermomechanical processing have also been shown to influence the damping capacity of the material. Finally, the ability to transmit energy from the vibrating object to the SMA is crucial, and some damping applications have failed due to their inability to do so.

Yoshida et. al.<sup>4,5</sup> investigated NiTi and also ternary NiTiCu, which has a higher transformation temperature due to the Cu content. Elevated damping occurred over a temperature range of approximately 200-300K for the materials in the study. The peak loss factor was as high as 0.18. This study indicated the nature of two different damping peaks. One peak was attributed to the martensite transformation, was dependent on frequency, and was observed to decrease with time under isothermal conditions. A second more stable peak was attributed to the R-phase transformation, which only occurred under certain heat treatments.

Coluzzi et. al.<sup>6</sup> studied the damping of NiTi and NiTiCu alloys under various thermomechanical treatments and hydrogen-doping. The hydrogen-doping introduced damping peaks that were insensitive to the test frequencies between 1 Hz and 3.5 kHz.

Although the damping levels of these materials are impressive, the damping peaks occurred near or below room temperature, making them unsuitable for most aircraft engine applications.

### 1.3 NASA GRC high-temperature shape memory alloy research

Noebe et. al.<sup>7,8</sup> have reported on new NASA GRC-developed ternary shape memory alloy formulations for high-temperature operation, including NiPdTi and NiPtTi. Recently, Padula et. al.<sup>9</sup> described a NiTiPdPt alloy with a transformation temperature near 300°C for high-temperature turbomachinery applications. The NASA GRC research has primarily supported the application of HTSMAs as actuators; the damping properties have not been investigated prior to this study.

The focus of this effort is on two different NiTiHf compositions – extruded  $Ni_{50}Ti_{35}Hf_{15}$  and cast  $Ni_{49.5}Ti_{35.5}Hf_{15}$ . Initial modulus testing showed the phase transformation temperatures occurring over a large temperature range. While this makes the materials less suitable for shape memory actuation, it was thought that it might yield elevated damping over a wider temperature range, making the materials more viable for use in applications where the temperature is not well-controlled. Additionally, the high phase transformation temperatures make these materials better suited for use in certain parts of an aircraft engine (e.g. fan or compressor).

## 2. APPROACH

Potential damping materials for turbomachinery applications undergo a process of analysis and testing at NASA GRC. Tasks include:

- Required material properties – Utilize finite element analysis (FEA) to determine the loss factor required of a material for use in a particular application. In this case the application is a titanium alloy beam typically used for vibration testing, with a SMA material placed in a layer on the beam surface.
- Material properties testing – Measure the loss factor and Young’s modulus of the damping material as functions of temperature, frequency, and strain amplitude. Determine whether it is a viable candidate for the application.
- FEA enhancement – Implement material properties in the FEA to include dependence on temperature, frequency, and strain level. Predict structure damping under environmental conditions, including high temperature and centrifugal loading.
- Structure vibration testing – Fabricate the beam structure with the damping material attached or embedded. Perform vibration testing to determine the loss factor of the structure to compare with the undamped baseline structure. Validate FEA with test results.
- Environmental vibration testing – Perform structure vibration testing under typical engine conditions. This includes high temperature testing and testing under centrifugal loads. Compare results to FEA predictions under environmental conditions.

This report will give results for the first two tasks outlined above. Some data for a simple FEA of a beam with SMA damping layers is included. Finally, the material properties of the HTSMAs at various temperatures and frequencies are presented.

## 3. REQUIRED MATERIAL PROPERTIES

### 3.1 Aircraft engine application

The target application for this work is a titanium-alloy cold-side compressor blade, which operates at temperatures ranging up to 300°C. Vibratory strain amplitudes can reach  $10^{-3}$ . Due to centrifugal loading, static strains can range from zero at the blade tip, to on the order of  $10^{-3}$  within the blade. Frequencies are on the order of 100 to 10,000 Hz.

Lazan<sup>10</sup> reported that a titanium alloy such as Ti-6Al-4V has a material loss factor  $\eta$  of  $2.5 \times 10^{-3}$  at 15 Hz,  $7.0 \times 10^{-4}$  at 100 Hz, and  $5.0 \times 10^{-5}$  at 1500 Hz. The loss factor  $\eta$  of a material is the ratio of damping energy to strain energy, or  $\eta = D/(2\pi U)$ , where  $D$  is the energy dissipated and  $U$  is the unit strain energy at maximum strain. The loss factor is equal to the inverse of the quality factor  $Q$ , twice the damping coefficient  $\zeta$ , and is equal to the loss tangent  $\tan \delta$  reported by other researchers; or  $\eta = Q^{-1} = 2\zeta = \tan \delta$ .

The blade itself can have a higher structure loss factor than that of the material. The blade structure loss factor is typically on the order of  $10^{-3}$  or less, depending on the vibration mode, but  $10^{-2}$  or more would be desirable for resonant stress reduction. This can be accomplished by incorporating a high damping material within or on the surface of the blade. However, if the damping material is placed on the blade surface, it needs to be very thin so that it does not adversely affect the aerodynamics. Thus, a thickness of 0.13mm (0.005 in) or less would be preferred.

### 3.2 Required loss factor

To determine the SMA loss factor necessary for successful structure damping, an analysis of a titanium alloy Ti-6Al-4V beam with SMA damping layers was performed. This beam type has been used in the past for testing various damping concepts. It has bending resonance frequencies that are in the range of turbomachinery blades (45 Hz up to 1000’s of Hz), and can show the effects of damping treatments on multiple mode shapes and frequencies.

The Oberst beam equations<sup>11</sup> give the structure loss factor of a simply supported beam with a damping layer. For a thin layer, the equations show that the structure loss factor depends on the product of the layer-to-beam modulus ratio and the layer-to-beam thickness ratio, or  $(E_{SMA}/E_{beam}) \cdot (t_{SMA}/t_{beam})$ . The larger this product is, the higher the structure loss factor will be. In addition, the structure loss factor is directly proportional to the damping layer loss factor,  $\eta_{SMA}$ .

In addition to using the Oberst equations, a finite element analysis (FEA) was performed on the beam using ANSYS Workbench. The beam is clamped at one end, with exposed dimensions of 203 mm long, 19 mm wide, and 2.3 mm thick (8.0 in x 0.75 in x 0.09 in). Figure 2 shows the beam and the FEA results for relative strain levels in its third bending vibration resonance mode. In past testing of the third bending mode of the plain undamped beam, the beam-alone loss factor,  $\eta_{\text{beam}}$ , was found to be about 0.002, and this was used as the baseline in the FEA.

The beam was analyzed with a 0.13-mm (0.005-in) thick SMA damping layer on both sides. The Young’s modulus of the SMA was set at 80GPa, Poisson’s ratio was 0.33, and the density was 8 g/cm<sup>3</sup>. In the FEA, an acceleration excitation was placed over the entire beam to simulate vibration testing, and the displacement of the beam tip was determined. Figure 3 shows the beam tip response as a function of excitation frequency for two values of SMA loss factor,  $\eta_{\text{SMA}}$ . Clearly a high  $\eta_{\text{SMA}}$  will dramatically reduce the beam response, resulting in lower vibratory stresses within the beam. The loss factor of the SMA-damped beam structure,  $\eta_{\text{st}}$ , was calculated from the frequency response of the beam tip. Figure 4 shows  $\eta_{\text{st}}$  as a function of  $\eta_{\text{SMA}}$  for both the ANSYS results and calculated from the Oberst equations. The target  $\eta_{\text{st}}$  of  $10^{-2}$  was predicted to be possible with a  $\eta_{\text{SMA}}$  of approximately 0.04.

Another scenario involves placing a smaller SMA patch on the beam to directly target a particular mode. Figure 2(b) shows a SMA patch placed in an area of high strain for the third bending mode. A FEA was performed with SMA patches, 51 mm x 19 mm x 0.25 mm (1.8 in x 0.75 in x 0.010 in), placed on the top and bottom of the beam, centered at 58 mm (2.3 in) from the tip. A value for  $\eta_{\text{SMA}}$  of 0.07 yielded the target  $\eta_{\text{st}}$  of  $10^{-2}$  for the third bending mode.

In this simple FEA, the SMA loss factor and other properties were assumed to be constant. Clearly, the loss factor and Young’s modulus of a SMA will be nonlinear. However, this analysis indicates the magnitude of SMA loss factor necessary to achieve the desired structure damping.

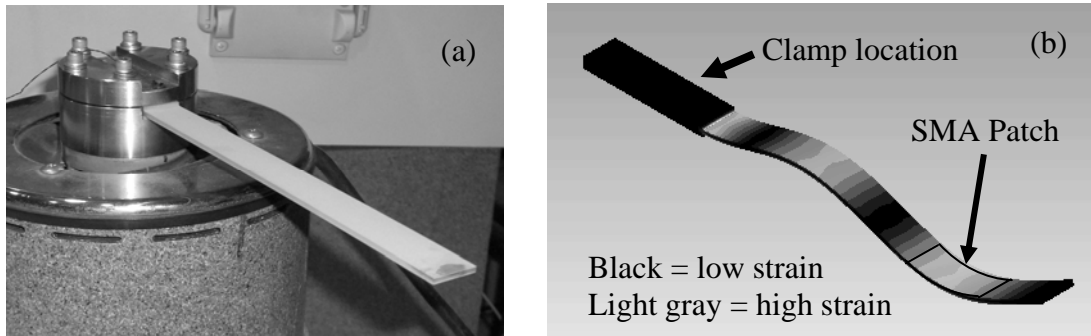


Fig. 2. (a) Typical test beam on vibration exciter. (b) FEA result, third bending mode strain, cantilever beam, shown with SMA patch targeting third mode.

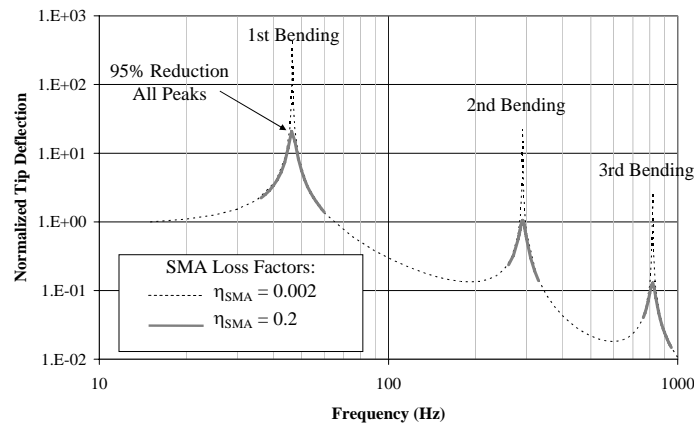


Fig. 3. FEA results for beam tip response versus excitation frequency. Effect of SMA loss factor on beam structure response, beam with 0.13mm SMA layers on both sides, beam alone loss factor  $\eta_{\text{beam}} = 0.002$ .

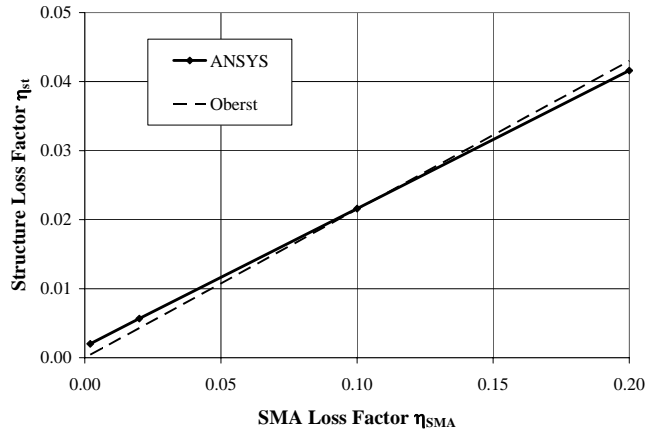


Fig. 4. Damped beam  $\eta_{st}$  versus SMA material  $\eta_{SMA}$ , beam with 0.13mm SMA layers on both sides. ANSYS result – beam alone loss factor  $\eta_{beam} = 0.002$ , Oberst result – beam alone loss factor  $\eta_{beam} = 0$ .

## 4. MATERIAL PROPERTIES TESTING

### 4.1 NiTiHf Materials

The HTSMAs investigated here are two samples each of  $Ni_{50}Ti_{35}Hf_{15}$  and  $Ni_{49.5}Ti_{35.5}Hf_{15}$ . The  $Ni_{50}Ti_{35}Hf_{15}$  alloy was cast, then extruded and machined to the final nominal dimensions of 55mm x 6.3mm x 1mm and 55mm x 6.3mm x 1.3mm. The  $Ni_{49.5}Ti_{35.5}Hf_{15}$  alloy was tested as-cast, both samples machined to the final nominal dimensions of 55mm x 8mm x 1mm. These materials undergo a single-step transformation from B2 austenite to B19 (orthorhombic) martensite.

The NiTiHf alloys were chosen because they exhibited a wide transformation hysteresis. It was thought that this temperature difference would allow a larger temperature range over which the elevated damping might occur.

### 4.2 DMA test procedure

The samples were tested on a TA Instruments dynamic mechanical analyzer (DMA), model 2980. In one test, the transformation temperatures  $M_f$ ,  $M_s$ ,  $A_s$ , and  $A_f$  were measured with a static loading test. The samples were held in three-point bending while a constant force of 15 N acted on the center of each specimen. The samples went through two cycles of heating and cooling from room temperature (or below) to 300°C, at 5°C per minute, with results given for the second cycle. The deflection of the sample at the center point was measured as a function of temperature.

In a second test, an alternating force was applied to the center of each sample, with the strain amplitude controlled to a prescribed value of  $34\text{--}35 \times 10^{-6}$ . The DMA measured Young's modulus and loss factor of each sample, under conditions of zero static strain, from room temperature to 300°C. Two cycles of both heating and cooling at 5°C per minute were conducted for frequencies ranging from 0.1 to 100 Hz.

The DMA used here was limited to frequencies at or below 200 Hz. Although the frequencies tested are lower than expected for the turbomachinery blade application, the well-controlled DMA measurements should give a good indication of the trends in damping as functions of frequency and temperature.

### 4.3 DMA results – cast $Ni_{49.5}Ti_{35.5}Hf_{15}$

The static results for the two cast  $Ni_{49.5}Ti_{35.5}Hf_{15}$  samples are shown in Figure 5. The deflection at the center of the sample is displayed as a function of temperature. It is assumed that the difference between the two samples is due to slightly different exposed lengths between the DMA clamps, since the sample dimensions are the same. The arrows indicate the direction of heating or cooling. The transformation temperatures are approximately  $M_f = 100^\circ\text{C}$ ,  $M_s = 140^\circ\text{C}$ ,  $A_s = 200^\circ\text{C}$ , and  $A_f = 210^\circ\text{C}$ .

Figure 6 shows dynamic test results for one sample at 0.1 Hz with strain amplitude of  $35 \times 10^{-6}$ . The second sample had very similar results. The loss factor reaches a peak of about 0.2 in heating and cooling. The temperature at which these peaks occur are quite different; in heating the peak occurs at 200°C, and in cooling the peak occurs at 125°C.

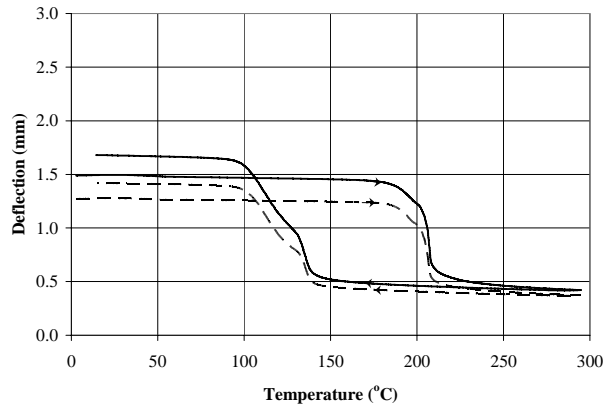


Fig. 5. DMA static test – cast  $\text{Ni}_{49.5}\text{Ti}_{35.5}\text{Hf}_{15}$  – deflection as a function of temperature for two samples.

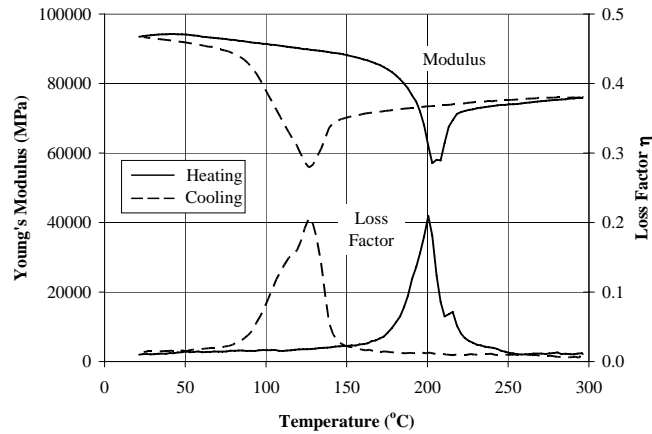


Fig. 6. Cast  $\text{Ni}_{49.5}\text{Ti}_{35.5}\text{Hf}_{15}$  modulus and loss factor versus temperature, effect of heating and cooling, 0.1 Hz,  $35 \times 10^{-6}$  strain amplitude.

The damping peaks correlate well with the phase transformation regions, as shown in Figure 7. Here the static and dynamic test results are plotted together. This indicates that the peak damping occurs only in the region where the material is transforming from one phase to the other, meaning that the breadth of the hysteresis envelope may be less important than originally envisioned. In fact, the large hysteresis may actually be problematic as damping occurs at different temperatures depending on whether the system is in the process of heating or cooling. This makes design with the alloy more complex and less desirable, as the properties are shifted rather than coincident.

Figure 8 shows the effect of frequency on the loss factor in heating. The data for cooling is given in Figure 9. There is a marked effect of frequency on the loss factor of this material. The peak loss decreases with increasing frequency, with no noticeable peak at 100 Hz. The literature indicates that this type of frequency-dependence is typical of the B2-B19 transformation.

With regard to the beam application, the first bending mode is at 45 Hz. Based on the loss factors presented in Figures 8 and 9, the SMA damping is negligible at the frequencies required for the blade application. Thus, unless future tests show that damping is higher for higher static strain levels, this particular alloy will be considered inappropriate for damping of turbomachinery blades, which require even higher frequencies.

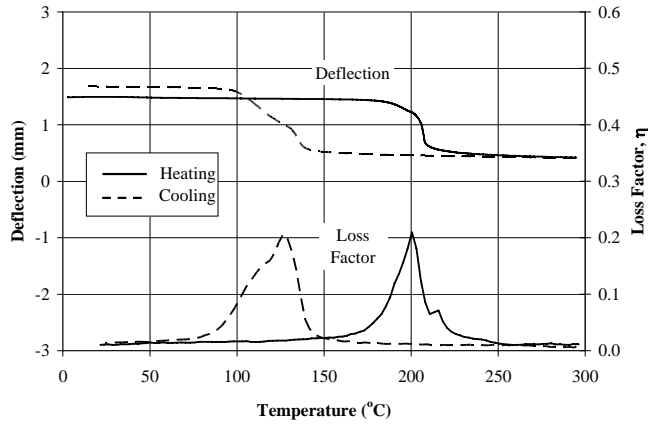


Fig. 7. Cast  $\text{Ni}_{49.5}\text{Ti}_{35.5}\text{Hf}_{15}$  static test deflection and dynamic test loss factor versus temperature. Loss factor at 0.1 Hz,  $35 \times 10^{-6}$  strain amplitude.

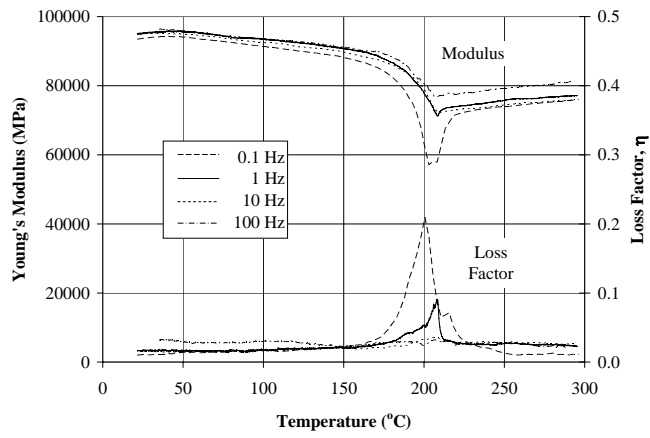


Fig. 8. Cast  $\text{Ni}_{49.5}\text{Ti}_{35.5}\text{Hf}_{15}$  modulus and loss factor versus temperature, effect of frequency,  $35 \times 10^{-6}$  strain amplitude, heating only.

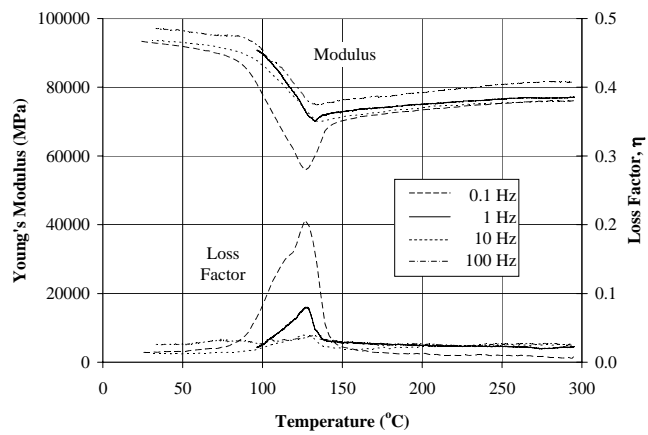


Fig. 9. Cast  $\text{Ni}_{49.5}\text{Ti}_{35.5}\text{Hf}_{15}$  modulus and loss factor versus temperature, effect of frequency,  $35 \times 10^{-6}$  strain amplitude, cooling only.

#### 4.4 DMA results – extruded Ni<sub>50</sub>Ti<sub>35</sub>Hf<sub>15</sub>

Figure 10 shows the results of the static test for the extruded Ni<sub>50</sub>Ti<sub>35</sub>Hf<sub>15</sub> samples. Again, the M<sub>f</sub>/M<sub>s</sub> temperatures are much lower than the A<sub>s</sub>/A<sub>f</sub> temperatures; however, both the forward and reverse transformations occurred over a narrower temperature range than for the cast Ni<sub>49.5</sub>Ti<sub>35.5</sub>Hf<sub>15</sub> samples. Based on the 1.0-mm thick sample, the transformation temperatures are approximately M<sub>f</sub> = 45°C, M<sub>s</sub> = 50°C, A<sub>s</sub> = 127°C, and A<sub>f</sub> = 132°C. The 1.3-mm thick sample deflected less than the 1.0-mm thick sample. This is expected since the sample stiffness increases with thickness, and both samples were loaded with the same 15-N force.

Dynamic test results for the 1.3-mm thick extruded Ni<sub>50</sub>Ti<sub>35</sub>Hf<sub>15</sub> sample at 0.1 Hz with strain amplitude of 34x10<sup>-6</sup> are shown in figure 11. The loss factor reaches a peak of 0.26 in heating. The peak loss factor in cooling was lower; however, with M<sub>f</sub> near the low end of the test temperature range, the entire peak may not have been captured. The temperature at which these peaks occur are quite different (in heating the peak occurs at 125°C, and in cooling the peak appears to be at approximately 40°C or lower), again indicating that wide hysteresis is not desirable.

Figure 12 gives the static test results with the 0.1-Hz dynamic test results. The damping peaks are located only in the regions where the transformation is taking place.

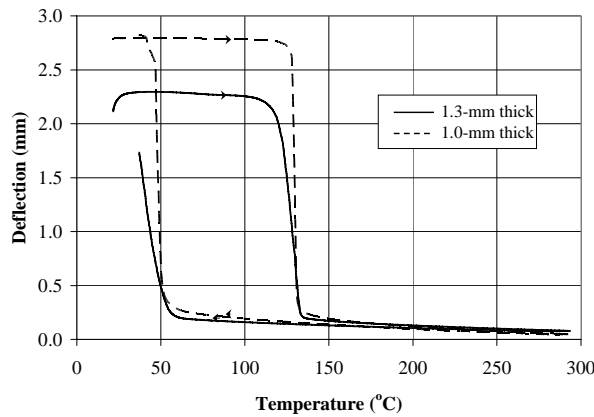


Fig. 10. DMA static test – extruded Ni<sub>50</sub>Ti<sub>35</sub>Hf<sub>15</sub> – deflection as a function of temperature for two sample thicknesses.

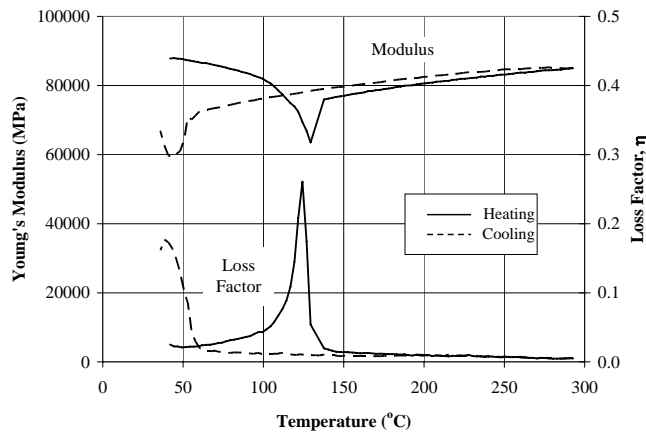


Fig. 11. Extruded Ni<sub>50</sub>Ti<sub>35</sub>Hf<sub>15</sub> modulus and loss factor versus temperature, 0.1 Hz, 34x10<sup>-6</sup> strain amplitude, effect of heating and cooling, 1.3-mm thick sample.

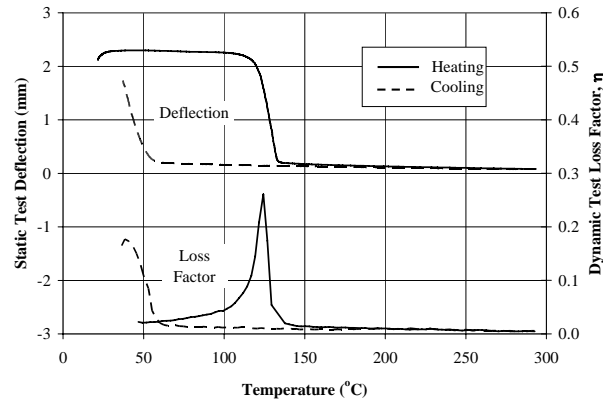


Fig. 12. Extruded  $\text{Ni}_{50}\text{Ti}_{35}\text{Hf}_{15}$  static test deflection and dynamic test loss factor versus temperature, 1.3-mm thick sample. Loss factor at 0.1 Hz,  $34 \times 10^{-6}$  strain amplitude.

Figure 13 shows the effect of frequency on the loss factor for extruded  $\text{Ni}_{50}\text{Ti}_{35}\text{Hf}_{15}$  in heating. Again, the peak loss decreases with increasing frequency, with no noticeable peak at 100 Hz. The results in cooling appear to show the same behavior; however, the peaks were not fully captured within the testing temperature range. Again, since the damping at higher frequencies was very low, this alloy will probably be a poor choice for the turbomachinery application.

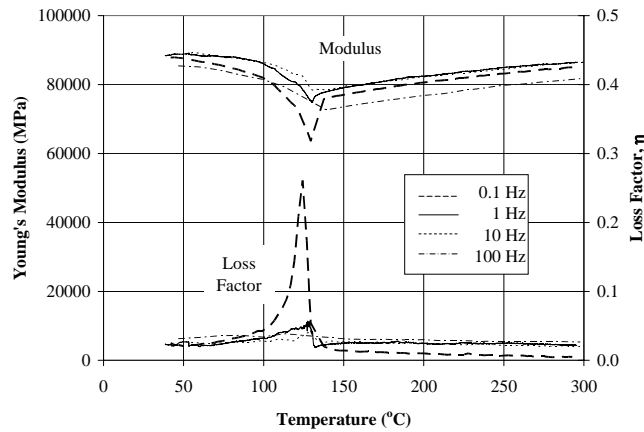


Fig. 13. Extruded  $\text{Ni}_{50}\text{Ti}_{35}\text{Hf}_{15}$  modulus and loss factor versus temperature, effect of frequency,  $34 \times 10^{-6}$  strain amplitude, heating only, 1.3-mm thick sample.

## 5. CONCLUSION

Results show that damping peaks coincided with the martensite/austenite phase transformation regions. Peak loss factors of over 0.2 occurred at the lowest frequency tested, 0.1 Hz. This is well above the 0.04 loss factor required for the beam vibration application. However, the peak damping decreased with increasing frequency, with no noticeable damping peak at 100 Hz. The peak loss factor occurred at higher temperatures when tested in heating as opposed to cooling. Therefore, in terms of the turbomachinery blade application, there are issues with these particular alloys, namely:

- Temperature hysteresis – It was initially thought that having the phase transformation temperatures far apart might yield elevated damping over a wide temperature range. However, damping peaks occurred about 75-100°C apart in heating and cooling, without overlap. Thus, it may be preferable to have minimal temperature hysteresis with all transformation temperatures well above room temperature. In addition, wider damping peaks would be preferred to allow damping over a broader temperature range.

- Frequency dependence – The damping peaks appear to be caused by the B2-B19 phase transformation, with its frequency-dependence. Although the damping was high at 0.1 Hz, the turbomachinery application requires damping at frequencies on the order of 100 to 10,000 Hz. A better material choice might have an additional phase transformation causing damping that is insensitive to frequency, similar to the R-phase in the binary NiTi alloy.

Since the results obtained from the ternary NiTiHf alloys did not exhibit all of the desired properties for the blade application, additional work is necessary. Identification of HTSMA candidates with low hysteresis and less frequency-dependence is required. However, it is unclear whether these desired properties are best obtained through alloy or processing modifications.

In addition, as more suitable materials are identified, future testing will include testing at higher frequencies and at steady-state and dynamic strain levels each up to  $10^{-3}$  to simulate conditions in a rotating engine blade.

In conclusion, a peak loss factor of 0.04 or greater would be sufficient for the turbomachinery blade application. Testing of the NiTiHf alloys showed that this loss factor could be achieved under certain conditions. More testing must be performed on HTSMA candidate materials to identify an alloy that will provide comparable or better damping under real turbomachinery blade conditions.

## REFERENCES

- <sup>1</sup> Y. El-Aini, R. deLanville, A. Stoner, and V. Capece, "High cycle fatigue of turbomachinery components – industry perspective," AIAA-1997-3365 (1997).
- <sup>2</sup> Y. Sherwin and D. G. Ulmer, "Method for vibration damping using superelastic alloys," United States Patent 6,796,408 (2004).
- <sup>3</sup> J. Van Humbeeck, "Damping capacity of thermoelastic martensite in shape memory alloys," *Journal of Alloys and Compounds* **355(1)**, 58-64 (2003).
- <sup>4</sup> I. Yoshida, D. Monma, K. Iino, K. Otsuka, M. Asai, and H. Tsuzuki, "Damping properties of  $Ti_{50}Ni_{50-x}Cu_x$  alloys utilizing martensitic transformation," *Journal of Alloys and Compounds* **355(1)**, 79-84 (2003).
- <sup>5</sup> I. Yoshida and K. Otsuka, "Effect of heat treatments on the damping characteristics of TiNi-based shape memory alloys," *Key Engineering Materials* **319**, 33-38 (2006).
- <sup>6</sup> B. Coluzzi, A. Biscarini, G. Mazzolai, F. M. Mazzolai, A. Tuissi, and E. Villa, "Damping properties of vacuum annealed and H-doped NiTi based alloys at low stress amplitudes," *Key Engineering Materials* **319**, 1-8 (2006).
- <sup>7</sup> R. Noebe, S. Padula II, G. Bigelow, O. Rios, A. Garg, and B. Lerch, "Properties of a  $Ni_{19.5}Pd_{30}Ti_{50.5}$  high-temperature shape memory alloy in tension and compression," *Proceedings of Smart Structures and Materials 2006: Active Materials: Behavior and Mechanics* **6170** (2006).
- <sup>8</sup> R. Noebe, D. Gaydosh, S. Padula II, A. Garg, T. Biles, and M. Nathal, "Properties and potential of two (NiPt)Ti alloys for use as high-temperature actuator materials," *Proceedings of Smart Structures and Materials 2005: Active Materials: Behavior and Mechanics* **5761**, 364-375 (2005).
- <sup>9</sup> S. Padula II, R. Noebe, G. Bigelow, D. Culley, M. Stevens, N. Penney, D. Gaydosh, T. Quackenbush, and B. Carpenter, "Development of a HTSMA-actuated surge control rod for high-temperature turbomachinery applications," AIAA-2007-2196 (2007).
- <sup>10</sup> B. J. Lazan, *Damping of Materials and Members*, Pergamon Press, Oxford, 1968.
- <sup>11</sup> A. D. Nashif, D. I. G. Jones, and J. P. Henderson, *Vibration Damping*, John Wiley and Sons, New York, 1985.